

Article

Impact of Three Gorges Reservoir Water Impoundment on Vegetation–Climate Response Relationship

Mengqi Tian ^{1,2} , Jianzhong Zhou ^{1,2,*}, Benjun Jia ^{1,2} , Sijing Lou ^{1,2} and Huiling Wu ^{1,2}

¹ School of Hydropower and Information Engineering, Huazhong University of Science and Technology, Wuhan 430074, China; tmq@hust.edu.cn (M.T.); jbj@hust.edu.cn (B.J.); d201880944@hust.edu.cn (S.L.); wuhuiling@hust.edu.cn (H.W.)

² Hubei Key Laboratory of Digital Valley Science and Technology, Wuhan 430074, China

* Correspondence: jz.zhou@hust.edu.cn; Tel.: +86-136-0717-4132

Received: 13 July 2020; Accepted: 31 August 2020; Published: 3 September 2020



Abstract: In recent years, the impact of global climate change and human activities on vegetation has become increasingly prominent. Understanding vegetation change and its response to climate variables and human activities are key tasks in predicting future environmental changes, climate changes and ecosystem evolution. This paper aims to explore the impact of Three Gorges Reservoir (TGR) water impoundment on the vegetation–climate response relationship in the Three Gorges Reservoir Region (TGR) and its surrounding region. Firstly, based on the SPOT/VEGETATION NDVI and ERA5 reanalysis datasets, the correlation between climatic factors (temperature and precipitation) and NDVI was analyzed by using partial correlation coefficient method. Secondly, nonlinear fitting method was used to fit the mapping relationship between NDVI and climatic factors. Then, the residual analysis was conducted to evaluate the impact of TGR impoundment on vegetation–climate response relationship. Finally, sensitivity index (SI), sensitivity variation index (SVI) and difference index (DI) were defined to quantify the variation of vegetation–climate response relationship before and after water impoundment. The results show that water impoundment might have some impacts on the response of vegetation–climate, which gradually reduced with increasing distance from the channel; comparing with the residual analysis method, the SI and DI index methods are more intuitive, and combining these two methods may provide new ideas for the study of the impact of human activities on vegetation.

Keywords: Three Gorges Reservoir; vegetation–climate relationship variation; water impoundment impact; NDVI; ERA5

1. Introduction

Vegetation, which plays a significant role in controlling desertification and conservation of soil and water [1], is an important component of terrestrial ecosystems and acts a pivotal part in climate change by affecting carbon storage, hydrological cycle and energy balance [2,3]. Therefore, vegetation coverage is an important indicator of ecological environment and global climate change [4–6]. For nearly half a century, the continuous impact of climate change and anthropogenic disturbances on global scale has become the main driving force for ecosystem change and has brought a huge impact on the vegetation ecosystem [7–9]. Undoubtedly, there is a close internal relationship between vegetation evolution and climate factors, but human activities can also interfere with vegetation evolution [4]. Understanding vegetation evolution and its response to climate change and human activities is a key task in predicting future ecosystem evolution, providing a basis for ecological management, ecosystem protection and decision-making [10–12].

The relationship between climate and vegetation has been widely discussed and studied by many scholars. Xu et al. [13] investigated the dynamic evolution of vegetation and its relations with climatic factors during 1982–2011 in China. They discovered that the spatiotemporal variations of vegetation dynamic evolution are controlled primarily by temperature and secondly by precipitation. However, the combined effects of temperature and precipitation exhibit strong spatial heterogeneity [14], and the complexity of the climate–vegetation relationship is also spatially and temporally variable [15]. For example, in northwestern China, the precipitation might be the key driving factor of vegetation growth [16], while, in Chinese Loess Plateau, the temperature is a main control factor of the seasonal change of vegetation and precipitation is an important factor for vegetation variation [17]. In addition, Xie et al. [18] showed temperature has a positive effect on vegetation in most periods in the semi-humid region but has no significant effect in the arid region, and precipitation has a positive effect on vegetation in summer in the arid region and in autumn in the semi-arid region. Because of the close relationship between climate and vegetation, the climate change inevitably has a certain impact on the vegetation ecosystem. Xu et al. [19] found that, from 1982 to 2000, global climate change has contributed to an increase in vegetation cover in the Qinghai-Tibet Plateau, and precipitation is the major climatic factor influencing interannual variation of average vegetation cover. Kong et al. [20] investigated vegetation response to climate change at Northern Hemisphere (NH) scale. Their research results show that factors potentially influencing vegetation growth in different parts of NH were complex and varied; for instance, temperature was recognized as the critical factor behind vegetation greenness in high latitudes especially for spring and autumn temperature in North America and Siberia. Additionally, some studies showed that vegetation changes and the response of vegetation to climate varied with seasons [18,21–23]. The relationship between vegetation and climate is not only the response of vegetation to climate, but also the impact of vegetation on regional climate. Some studies also indicated that vegetation impacts the regional climate by modulating the land–atmosphere exchanges of heat, water and momentum [24–26].

Human activities, which is another important factor affecting vegetation, should not be neglected in analyzing the vegetation dynamic evolution under the changing environment [18]. Zhang et al. [27] used the Carnegie–Ames–Stanford approach model to assess the status of vegetation in the Three-River Source Region across different periods from 1982 to 2012 and found that human activities had a weak negative impact from 1982 to 2000 and a favorable impact from 2001 to 2012 on vegetation growth or recovery. Hua et al. [28] found that land use change was the dominant factor driving long-term changes in vegetation greenness in China. Brandt et al. [29] reported that, in Sub-Saharan Africa, the increases in woody cover were associated with low population growth and were driven by increases in CO₂ in the humid zones and by increase in precipitation in drylands, whereas the decreases in woody cover were associated with high population growth. In addition, Li et al. [30] analyzed the main characteristics, spatial-temporal distribution and driving forces of vegetation restoration in the Shaanxi–Gansu–Ningxia Region, reporting that human activities are the main driving forces in vegetation restoration. For example, the “Grain for Green Project”, which turns cultivated land into forest land and aims to protect the ecological environment in China, was identified as the main cause leading to gradual vegetation stabilization in the Shaanxi–Gansu–Ningxia Region [31,32]. In addition to environmental protection projects, water conservancy project construction may also has an impact on vegetation. For example, Zhang et al. [33] analyzed the impact of the Three Gorges Water Conservancy Project on environment and reported that cropland, woodland and grassland areas reduced continuously, while river and built-up area increased from 2000 to 2005, and significant changes in land use and vegetation cover have occurred in the Three Gorges Reservoir (TGR) Area.

Climate change and human activities are the two main driving forces of vegetation cover change [4]. It is a key task to distinguish the effects of human activities and climate change on vegetation evolution for vegetation ecosystem protection and human activities impact assessment. The residual analysis method was firstly applied to discriminate between climate or human-induced dryland degradation by Evans et al. [34]. Then, this method began to be widely used to distinguish the impact of climate

and human activities on vegetation [35,36]. For example, Jiang et al. [37] used a residual analysis trend method to distinguish the effects of climatic change and human activities on vegetation evolution dynamics in Central Asia. Their research works highlighted that sparse vegetation and the degradation of some shrubs in the southern part of the Karakum Desert, the southern Ustyurt Plateau and the wetland delta of the Large Aral Sea were mainly triggered by human activities. Similarly, by using residual analysis, Sun et al. [38] found that human activities played a major role in vegetation variation of North China. In addition, based on residual analysis of NDVI variation, Wang et al. [39] pointed out that human activities had either improved or degraded vegetation cover in some parts in southern China. In theory, the residual analysis method is feasible, and establishing an ideal model of vegetation–climate is the key to identify the impact of human activities on vegetation. However, in practice, it is difficult to find the data without human intervention. Therefore, to overcome the shortcomings of residual analysis method, this study only investigated the impact of the TGR impoundment and did not consider other human activities. Then, a vegetation–climate model was established, which is not affected by impoundment, and the impact of water storage was studied by residual analysis.

The Three Gorges Water Conservancy Project at the upper end of the Yangtze River is currently the world's largest water conservancy project. Many studies in the Three Gorges Reservoir Region focused on the land use/cover changes [33] and the response of vegetation to natural and anthropogenic driving factors [40]. These studies did not pay attention to the impact of the Three Gorges Reservoir's impoundment. At present, there are few studies on the impact of TGR water impoundment on vegetation–climate relationship. Therefore, this study focused on vegetation–climate relationship and the impact of impoundment in different zones. The NDVI was chosen as a valid indicator for vegetation coverage variation, while precipitation and temperature were chosen as climate factors. The aims of this study were as follows: (1) to establish a vegetation–climate model and explore the relationship between them; (2) to propose a new method for analyzing the impact of water impoundment; (3) to quantify the impact of impoundment on climate–vegetation response relationship; and (4) to compare and verify the proposed new method with the existing method. Hopefully, knowledge of the vegetation variation and vegetation–climate relationship will promote the protection of the ecological environment in this region and manage ecosystem under the impacts of climate change and human activities.

2. Data and Methods

2.1. Study Area

The study area is the Three Gorges Reservoir Region (TGRR) and its 100-km buffer zone (Figure 1), which covers about 220,000 km². TGRR in this paper is a geographical region, which is located in the Cuntan-Yichang sub-catchment of the upper Yangtze River. The region of the TGRR is slightly different from the official TGRR, which is commonly defined as an administrative region containing 21 counties impounded by the Three Gorges Reservoir (TGR) [41]. Geographically, the TGRR is located at the junction of the Sichuan Basin and the middle and lower reaches of the Yangtze River. It crosses the mountainous canyons in Hubei and the ridge valleys in eastern Sichuan and is adjacent to Daba Mountain in the north and Hubei Plateau in Sichuan in the south. Its elevation is between –12 and 3070 m. The climate of the study area is a subtropical monsoon climate with an annual rainfall of 1000–1800 mm. The current land use types of the TGRR are farmland and forest (including secondary forest and virgin forest) that have resulted from long-term anthropogenic activity and a highly dense population [42].

The water level of TGR was raised from 66 to 135 m in June 2003, and reached the normal water level of 175 m for the first time in 2010. The impoundment of the TGR caused changes in the underlying surface along the river. The increase in water area will increase local evaporation and may cause changes in water vapor vertical movement of the Yangtze River's water vapor channel. It is likely to further change local climate and vegetation coverage in the TGRR and its buffer zone.

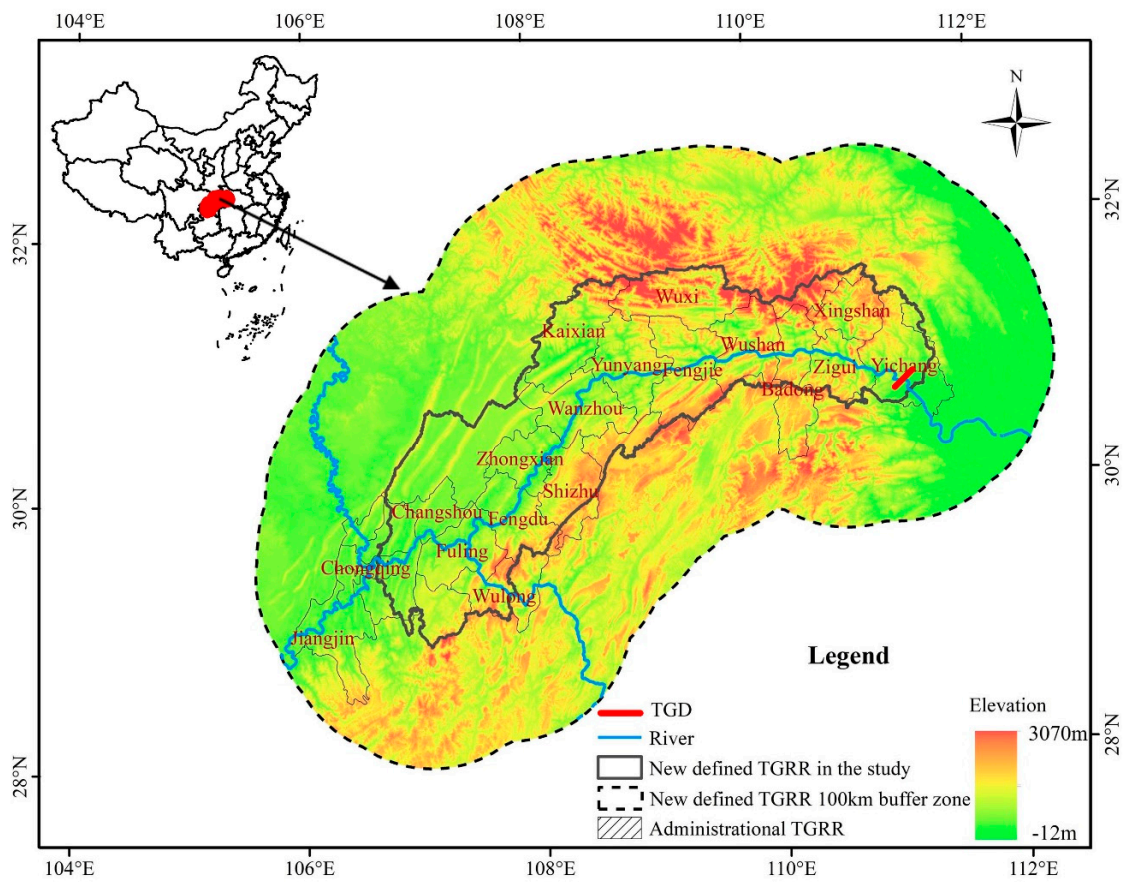


Figure 1. Geographic location and elevation of the study area.

2.2. Data

2.2.1. NDVI and Land Use/Land Cover Data

For ecologists, satellite remote sensing has become a potential goldmine for monitoring and predicting changes in vegetation activities over large regions in a repeatable manner [6,43,44], which is also widely used by climatologists [24–26,45–47] and researchers in natural disasters [48–50]. Normalized Difference Vegetation Index (NDVI), as an effective indicator to monitor vegetation and natural environment at regional and global scales, has been widely used in the research on vegetation activity [51–53]. The NDVI [54,55] is derived from the red, near-infrared reflectance ratio:

$$\text{NDVI} = (\text{NIR} - \text{RED}) / (\text{NIR} + \text{RED}) \quad (1)$$

where NIR and RED are the amounts of near-infrared and red light, respectively, reflected by the vegetation and captured by the sensor of the satellite.

The formula is based on the fact that chlorophyll absorbs RED, whereas the mesophyll leaf structure scatters NIR. NDVI values thus range theoretically from -1 to $+1$, where negative values correspond to an absence of vegetation [55].

NDVI can accurately reflect the surface vegetation coverage. In this study, 1998–2018 annual and monthly vegetation index datasets with a spatial resolution of 1 km were used, which are based on the continuous time series of SPOT/VEGETATION NDVI satellite remote sensing data using the maximum value composite method [56]. This dataset can effectively reflect the vegetation coverage distribution and change status in various regions of the country on space and time scales, and it is a very important reference for monitoring the changes of vegetation status, using vegetation resources reasonably and other research in related fields of ecological environment.

This study used land use/land cover data in 2000 and 2018 [57]. The land use/land cover data in 2000 and 2018 are based on Landsat-TM/ETM and Landsat 8 remote sensing image data, respectively. The classification system of land use/land cover data in China adopts a three-level classification system [58]. The first level, is divided into six categories based on land resources and their utilization attributes: arable land, forest land, grassland, water area, construction land and unused land. The second level is mainly classified according to the natural attributes of land resources, and the third level is mainly classified according to the topography of the arable land.

2.2.2. Meteorological Data

ERA5 [59] is the fifth generation ECMWF (European Centre for Medium-Range Weather Forecasts) atmospheric reanalysis of the global climate, and it will replace the ERA-Interim reanalysis, which is now 10 years old. Reanalysis combines model data with observations from across the world into a globally complete and consistent dataset using the laws of physics [59]. The 4D-Var assimilation method, which takes account of the exact timing of the observations and model evolution within the assimilation window, makes providing estimates worldwide for each hour of the day possible. This hourly output resolution is quite an improvement with respect to ERA-Interim and provides a more detailed evolution of particular weather events. Some researchers have compared and found that ERA5 shows improvements relative to ERA-Interim, which represents the previous generation reanalysis product [60–62]. For example, the precipitation and precipitable water vapor of ERA5 perform better than those of ERA-Interim in China [46,63,64], while the temperature difference between ERA5 and ERA-Interim is relatively smaller [65]. The ERA5 dataset has a time scale from 1979 to the present. The data format is a grid point with a spatial resolution of $0.25^\circ \times 0.25^\circ$. In this study, the precipitation and temperature data from 1998 to 2018 in the ERA5 dataset were used.

2.3. Methods

2.3.1. Partial Correlation Coefficient Method

In a multi-factor system, the partial correlation coefficient is used to study the influence or correlation of one factor to another factor and to exclude the influence of other factors in the process. This study used this method to analyze the correlation between the monthly NDVI and the monthly average temperature or monthly precipitation in each grid point. According to the definition, under the condition that the effect of z remains unchanged, the partial correlation coefficient between the variable x and the variable y is calculated as:

$$r_z^{xy} = \frac{r_{xy} - r_{xz}r_{yz}}{\sqrt{(1 - r_{xz}^2) + (1 - r_{yz}^2)}} \quad (2)$$

where r_{xy} , r_{xz} and r_{yz} , respectively, represent the Pearson correlation coefficient between the three variables x , y and z , and the calculation formula of the Pearson correlation coefficient of x and y is:

$$r_{xy} = \frac{\text{Cov}(x,y)}{\sqrt{\text{Var}(x)\text{Var}(y)}} = \frac{\sum_{t=1}^N (x_t - \bar{x})(y_t - \bar{y})}{\sqrt{\left[\sum_{t=1}^N (x_t - \bar{x})^2 \right] \left[\sum_{t=1}^N (y_t - \bar{y})^2 \right]}} \quad (3)$$

where N is the number of years, x_t is the value of the x -variable in the t th year, y_t is the value of the y -variable in the t th year, \bar{x} is the average of the x -variables in all years and \bar{y} is the average of the y -variables in all years.

2.3.2. Grid Point Analysis

The resolution of the vegetation index NDVI is 1 km × 1 km. When using 1 km × 1 km grid points as the benchmark units for statistical analysis, the large number of grid points will lead to long calculations. Therefore, based on weighing the calculation cost and accuracy, this study used 5 km × 5 km grid points as the benchmark analysis units. Interpolated NDVI, temperature and precipitation data to the grid by Inverse Distance Weight method. For the boundary grid processing, take those whose centroid is in the study area as benchmark analysis units. Thus, the research area is finally divided into 8933 benchmark statistical analysis units.

2.3.3. Establish Vegetation–Climate Regression Model

Regression model is a mathematical model that quantitatively describes statistical relationships. It studies the relationship between the dependent variable and the independent variable and can also show the strength of the influence of multiple independent variables on a dependent variable. Under the double effects of human activities and climate change, vegetation is constantly adapting to changes in external conditions to make its own activities more favorable. However, this process is dynamic and nonlinear, and it is necessary to further study this non-linear response relationship. In this paper, there are two independent variables (temperature and precipitation) and the dependent variable is NDVI. To express the nonlinear relationship between vegetation and climate, a polynomial regression model as shown in Equation (8) was selected.

$$z = p_0 + p_1x + \dots + p_nx^n + p_2y + \dots + p_my^m + p_3xy + \dots + p_ix^i y^j \quad (4)$$

where z represents dependent variable, x and y represent independent variables and p_0, \dots, p_i represent regression coefficients.

Before establishing the model, the correlations between NDVI and temperature/precipitation was analyzed. According to the results of partial correlation analysis, an appropriately simplified vegetation–climate regression model was established as Equation (5).

$$z = p_0 + p_1x + p_2y + p_3x^2 + p_4xy \quad (5)$$

where z represents NDVI, x represents temperature, y represents precipitation and p_0, p_1, p_2, p_3 and p_4 are regression coefficients.

After determining the regression model, the least squares method was used to fit the regression coefficients. Finally, residual sum of squares (SSE), coefficient of determination (R^2) and F-test were used to evaluate the fitting results.

2.3.4. Residual Analysis

The residual analysis approach, which can separate NDVI changes caused by human activities from those resulting from climatic variations, assumes that there is a strong relationship between vegetation production and climate [34]. First, the regression between NDVI and climatic factors (temperature and precipitation) is calculated in each zone. Second, the residual between the observed NDVI and the predicted NDVI is calculated. Finally, these residuals are regressed on time to obtain the trends. When the trend of NDVI residuals is insignificant, changes in NDVI are explained by climatic factors. In contrast, when the trend of NDVI residuals is significant, changes in NDVI are not explained by climatic factors and may have been caused by human activities. this study took June 2003 as the demarcation point of the water impoundment of TGR and established vegetation–climate models before and after impoundment. The precipitation and temperature data after impoundment were input into the regression model before impoundment to obtain the predicted NDVI. The residuals between the predicted value and the observed value were calculated. Since the impact of human activities such as environmental engineering and urbanization is continuous, it can be assumed that the

vegetation–climate relationships before and after impoundment are both affected by human activities. Therefore, the significant trend of NDVI residuals can be explained by impoundment.

2.3.5. Mann–Kendall Test

Mann–Kendall test (MK test) was first published by Mann [66], and then improved by Kendall [67]. It can effectively distinguish whether a natural process has certain trend or not. Suppose a time series is X_1, X_2, \dots, X_n ; construct MK test statistics S :

$$S = \sum_{i=1}^{n-1} \sum_{j=i+1}^n \text{sgn}(X_j - X_i) \quad (6)$$

where X_i and X_j represent the measured data of continuous time, n represents the length of the measured data and $\text{sgn}(\)$ is a symbolic function with the value:

$$\text{sgn}(\theta) = \begin{cases} 1 & \theta > 0 \\ 0 & \theta = 0 \\ -1 & \theta < 0 \end{cases} \quad (7)$$

Mann and Kendall proved that the statistical variable S obeyed an asymptotic normal distribution, and its expected and variance calculation formulas are:

$$\begin{aligned} E(S) &= 0 \\ \text{Var}(S) &= n(n-1)(2n+5)/18 \end{aligned} \quad (8)$$

In addition, the statistical variable Z is constructed in the following way:

$$Z = \begin{cases} \frac{S-1}{\sqrt{\text{Var}(S)}} & S > 0 \\ 0 & S = 0 \\ \frac{S+1}{\sqrt{\text{Var}(S)}} & S < 0 \end{cases} \quad (9)$$

Z follows the standard Gaussian distribution. If a significance level α is given, when $|Z| \geq Z_{1-\alpha/2}$, the null hypothesis is rejected, and the series has a significant trend. A positive (negative) Z value indicates that the sequence is increasing (declining). In this study, $\alpha = 0.05$, thus $Z_{1-\alpha/2} = 1.96$.

3. Results

3.1. Vegetation Evolution Pattern around the Reservoir

For each grid point, the annual maximum NDVI value from April 1998 to December 2018 was tested by Mann–Kendall method with a significance level of $\alpha = 0.05$ (Figure 2). The results show that, in study area, the grid points with significant increasing trend of NDVI accounted for 82.01%. The NDVI changes in 15.93% of the grid points were not significant, and the grid points with significant decreasing trend of NDVI accounted for 2.06%. NDVI changed insignificantly or decreased significantly in the areas which were mostly located in the densely populated Sichuan Basin or the lower reaches of the Yangtze River.

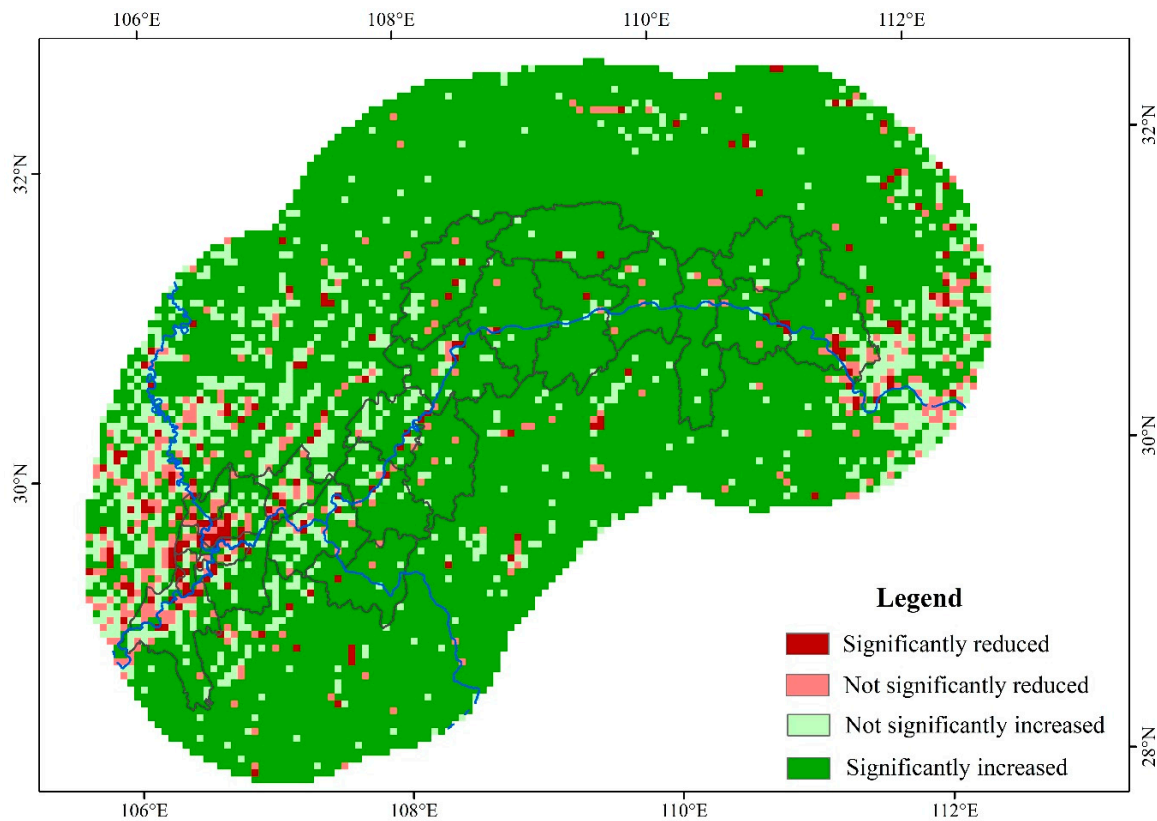


Figure 2. Trends of annual maximum NDVI from 1998 to 2018.

The land use/land cover of the study area in 2000 and 2018 are shown in Figure 3a,b, respectively. Compared with 2000, there was a significant increase in urban construction land in 2018, such as the Sichuan Basin, Chongqing and the middle and lower reaches of the Yangtze River.

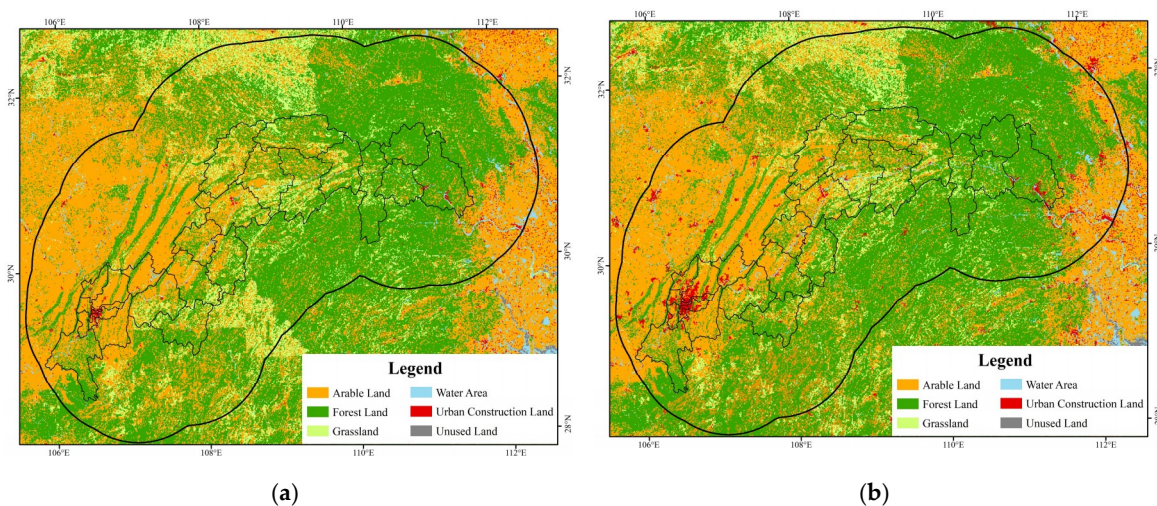


Figure 3. Land use/land cover changes in the study area: (a) land use/land cover in the study area in 2000; and (b) land use/land cover in the study area in 2018.

Comparing Figures 2 and 3, it is found that most of the areas where NDVI showed significant decreasing trends or insignificant trends are urban construction land or arable land. Many people live in urban construction land and arable land. Thus, human activities are relatively dense. In other words, intensive human activities may have some negative impacts on vegetation coverage.

In terms of time evolution, the annual NDVI of the study area from 1998 to 2018 was processed into areal means, and the results are shown in Figure 4. Since the NDVI changes showed a fluctuating rising trend and NDVI grew fastest in 2003, while the water impoundment level of the TGR increased from 66 to 135 m, it is speculated that the water impoundment of the TGR may have some impacts on its surrounding vegetation.

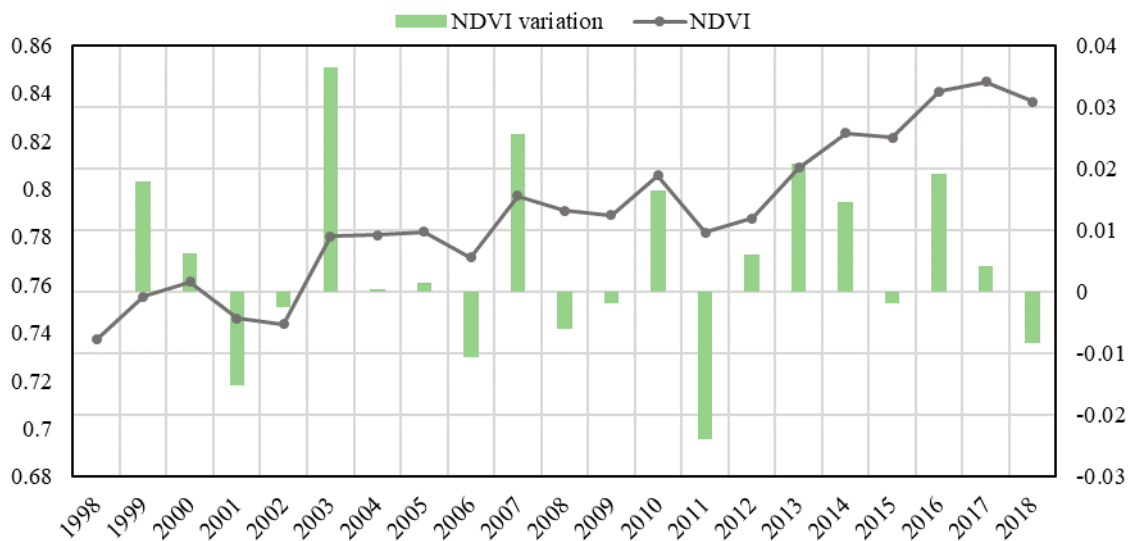


Figure 4. Areal mean change of annual NDVI from 1998 to 2018.

3.2. Screening the Drivers of Vegetation Change

The partial correlation coefficients between the monthly NDVI and the monthly average temperature, the monthly precipitation from April 1998 to December 2018 in the study area was calculated. The partial correlation coefficients of NDVI and temperature, which are referred to simply as r_{N-t} below, are shown in Figure 5a. Similarly, the partial relationship between precipitation and NDVI is abbreviated as r_{N-p} , and the results are shown in Figure 5b. It can be seen that, after excluding the influence of precipitation, r_{N-t} ranged from 0 to 0.87 and was generally high. Area with significant partial correlation ($|r_{N-t}| \geq 0.4$) accounted for 98.47% of the study area, with moderate partial correlation ($0.4 \leq |r_{N-t}| < 0.6$) accounting for 4.18%, high partial correlation ($0.6 \leq |r_{N-t}| < 0.8$) accounting for 82.93% and extremely high partial correlation ($|r_{N-t}| \geq 0.8$) accounting for 11.36%. Combining Figures 1, 3 and 5a, it can be seen that the areas with low partial correlation coefficients between temperature and NDVI were mainly located in the downstream of TGR, where human activities were relatively dense; the areas with high partial correlation coefficients were mostly located in mountainous areas and have less human activities. After excluding the influence of temperature, r_{N-p} was generally low, as shown in Figure 5b. r_{N-p} ranged from -0.39 to 0.26 , and no absolute value of partial correlation coefficient higher than 0.4 was found.

The monthly data of NDVI, temperature and precipitation were divided into four series: spring (March to May), summer (June to August), autumn (September to November) and winter (December to February). The correlation coefficients among NDVI, temperature and precipitation in each season were calculated. Figure 6 shows that r_{N-t} was high in spring and autumn and low in summer and winter. Combining Figures 3 and 6a,c, it can be seen that the areas with high correlation between temperature and NDVI in spring and autumn were concentrated in mountainous areas with less human activities, which were roughly similar to the high correlation area calculated from the total series. As shown in Figure 7, r_{N-p} was generally low in the four seasons. However, in summer and winter, the negative correlation between precipitation and NDVI in a few areas was slightly higher. The average r_{N-t} and r_{N-p} of the study area in the four seasons were calculated, as shown in Table 1. Comparing the results of the four seasons and the total series, it was found that the temperature and

NDVI correlation results in spring and autumn were very similar to the results of the total series. Whether comparing average values or percentages, the correlation between temperature and NDVI was higher than that between precipitation and NDVI in the four seasons.

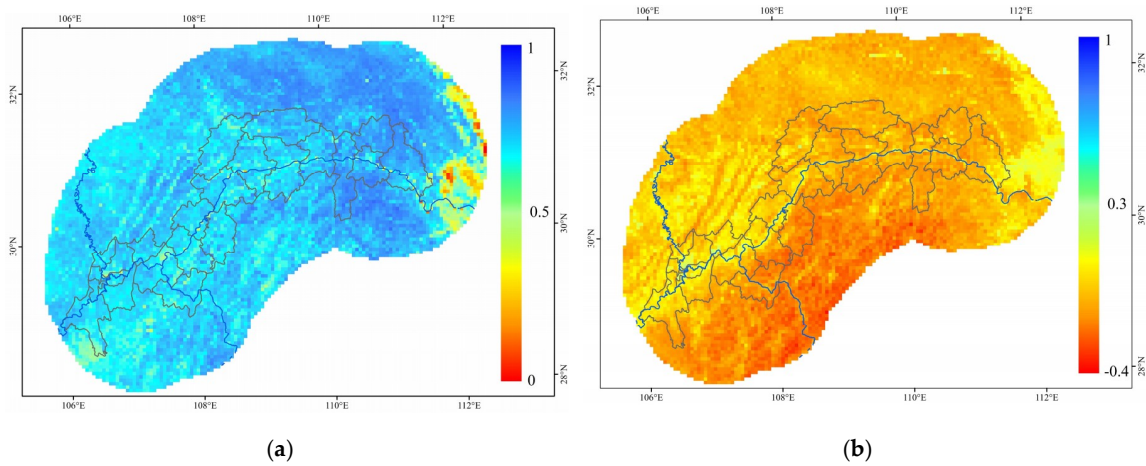


Figure 5. Partial correlation coefficient of NDVI–precipitation and NDVI–temperature (Total series). (a) partial correlation coefficient of NDVI–temperature; and (b) partial correlation coefficient of NDVI–precipitation.

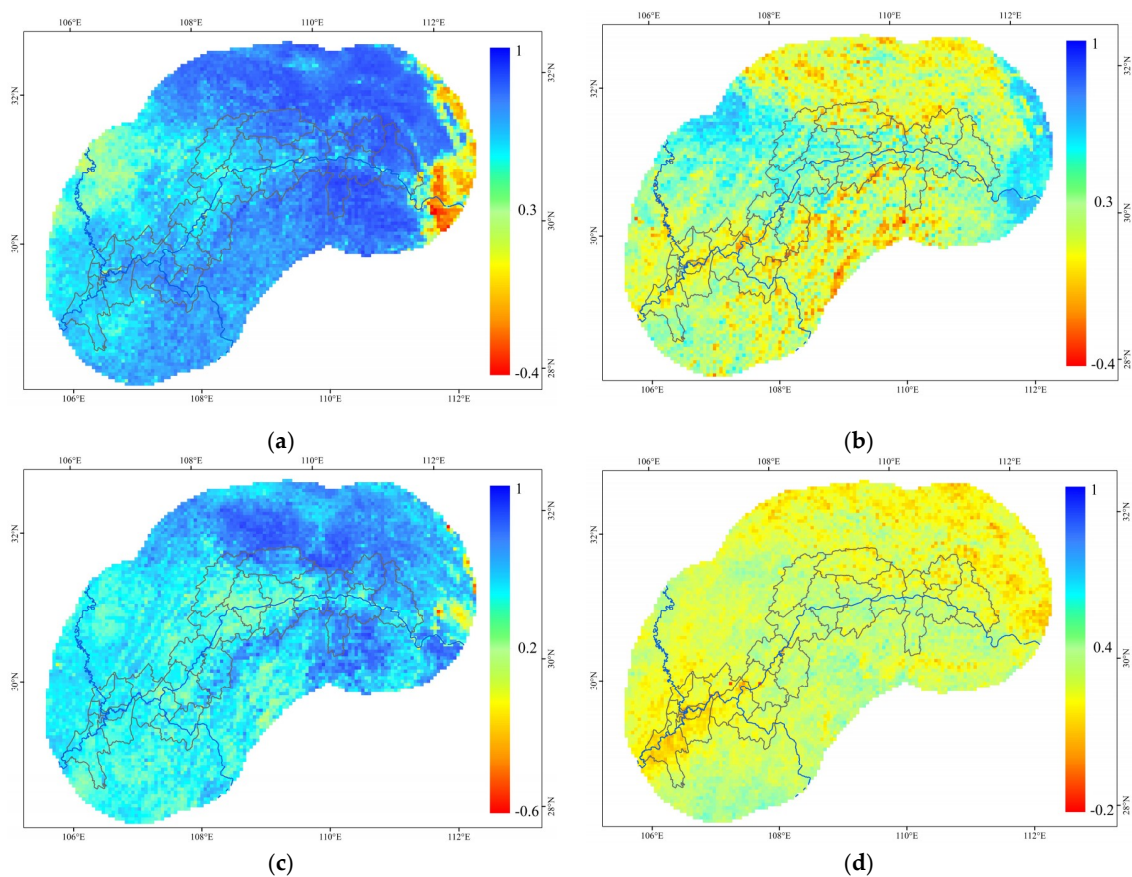


Figure 6. Partial correlation coefficient of NDVI–temperature in four seasons: (a) spring; (b) summer; (c) autumn; and (d) winter.

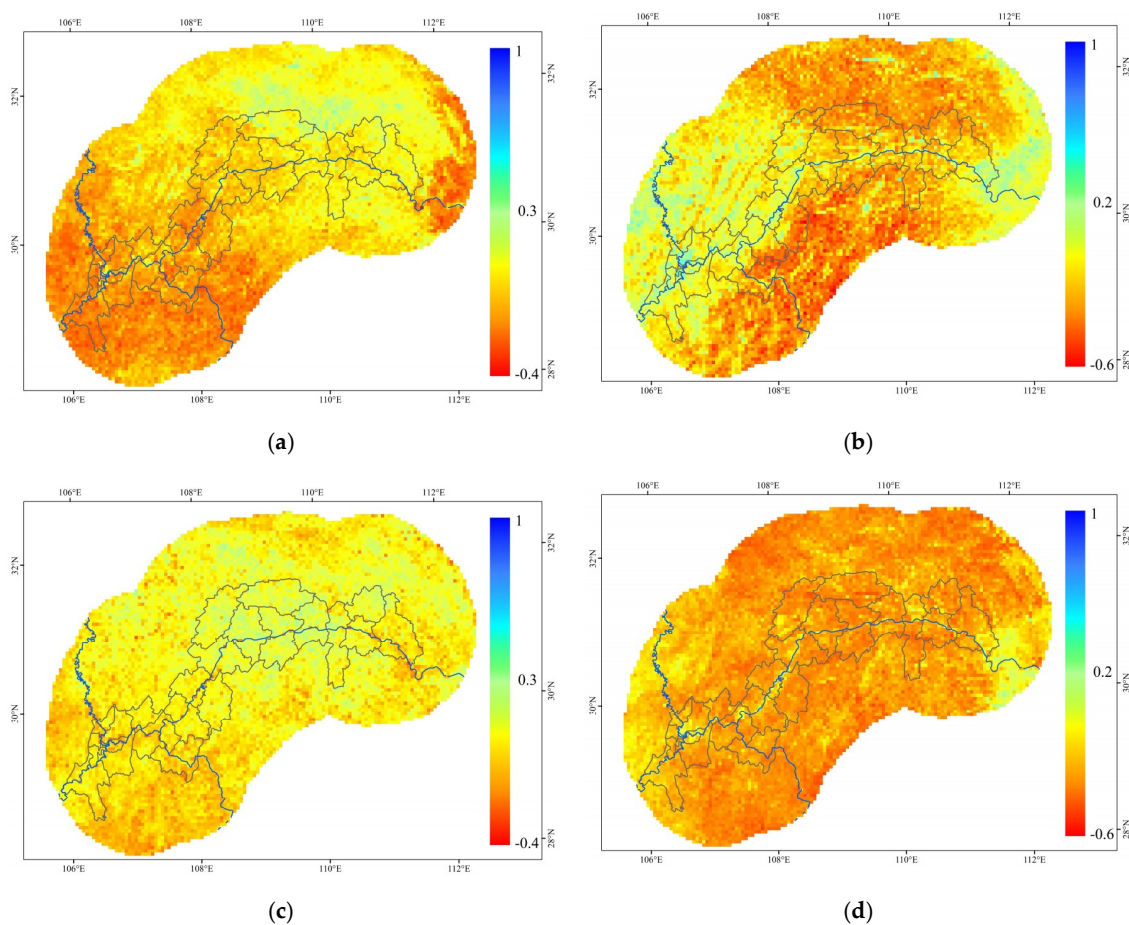


Figure 7. Partial correlation coefficient of NDVI–precipitation in four seasons: (a) spring; (b) summer; (c) autumn; and (d) winter.

Table 1. Average and percentage results of four seasons and total series.

| | Spring | Summer | Autumn | Winter | Total Series |
|------------------------------------|---------|---------|---------|---------|--------------|
| Average r_{N-t} | 0.654 | 0.268 | 0.532 | 0.295 | 0.718 |
| Percentage of $ r_{N-t} \geq 0.4$ | 92.086% | 23.699% | 83.231% | 10.075% | 98.47% |
| Average r_{N-p} | −0.037 | −0.163 | 0.057 | −0.282 | −0.090 |
| Percentage of $ r_{N-p} \geq 0.4$ | 0.034% | 9.874% | 0 | 9.123% | 0 |

In summary, the results show that the correlation between temperature and vegetation was stronger than that between precipitation and vegetation. Some studies used MODIS NDVI to conduct research in administrative TGR and found that the correlation between temperature and NDVI was stronger than that between precipitation and NDVI [68,69]. Temperature can be used as the main factor for vegetation change. In addition, the extent of partial correlation varies by region. That is, the dynamic vegetation–temperature and vegetation–precipitation responses had strong spatial heterogeneity, and there are some differences in the dynamic response relationship in different areas.

3.3. Vegetation–Climate Regression Model

The study presented in Section 3.2 showed that the correlation between temperature and NDVI was stronger than that between precipitation and NDVI. Therefore, temperature was considered as a main factor in the following study on the response of NDVI to climate. In addition, because of the strong spatial heterogeneity of the response, it was necessary to conduct divisional study. Based on the water–land boundary after impoundment of TGR, zones were divided every 10 km in the radial

direction. The monthly temperature and NDVI of each zone from April 1998 to December 2018 were extracted and averaged. Taking June 2003 as the demarcation point of the water impoundment of TGR, the least square method was used to fit the relationship between NDVI and temperature/precipitation before and after water impoundment. The regression coefficient results are shown in Table 2. The regression coefficients of different zones were different, and the regression coefficients before water impoundment are also different from those after water impoundment. However, the difference in regression coefficients caused by different zones was smaller than that caused by impoundment. From the evaluation index and p -value of Table 3, it can be seen that the regression model fitted well and passed the hypothesis test with significance level $\alpha = 0.01$. In other words, the multiple polynomial regression model established in this paper had good performance in fitting the relationship between vegetation and climate.

Table 2. Regression coefficients results of relationship between NDVI and climatic factors.

| Zones (km) | Before Impoundment | | | | | After Impoundment | | | | |
|---------------|--------------------|-------|------------------------|------------------------|------------------------|-------------------|-------|------------------------|------------------------|------------------------|
| | p_0 | p_1 | p_2 (10^{-5}) | p_3 (10^{-5}) | p_4 (10^{-6}) | p_0 | p_1 | p_2 (10^{-3}) | p_3 (10^{-4}) | p_4 (10^{-5}) |
| 0–10 | 0.160 | 0.026 | −1.176 | −25.1 | 4.764 | 0.212 | 0.040 | −1.136 | −8.252 | 5.065 |
| 10–20 | 0.179 | 0.025 | 1.871 | −20.29 | 1.527 | 0.239 | 0.041 | −1.288 | −8.385 | 5.578 |
| 20–30 | 0.209 | 0.023 | −2.125 | −10.44 | 1.035 | 0.259 | 0.039 | −1.278 | −7.8 | 5.457 |
| 30–40 | 0.217 | 0.022 | −2.628 | −6.946 | −0.329 | 0.264 | 0.038 | −1.231 | −7.227 | 5.175 |
| 40–50 | 0.218 | 0.022 | −12.73 | −7.649 | 3.68 | 0.255 | 0.038 | −1.298 | −7.168 | 5.442 |
| 50–60 | 0.220 | 0.023 | −14.48 | −8.769 | 4.098 | 0.258 | 0.037 | −1.261 | −6.909 | 5.274 |
| 60–70 | 0.228 | 0.022 | −18.55 | −7.109 | 5.334 | 0.261 | 0.036 | −1.21 | −6.593 | 5.072 |
| 70–80 | 0.223 | 0.021 | −18.27 | −4.098 | 5.491 | 0.255 | 0.035 | −1.15 | −6.115 | 4.889 |
| 80–90 | 0.236 | 0.021 | −18.96 | −3.693 | 5.806 | 0.266 | 0.035 | −1.087 | −5.861 | 4.53 |
| 90–100 | 0.225 | 0.021 | −14.87 | −3.966 | 4.28 | 0.256 | 0.035 | −1.075 | −5.848 | 4.444 |

Table 3. Evaluation index of fitting result.

| Zones | Before Impoundment | | | After Impoundment | | |
|--------|--------------------|----------------|--------------------------|-------------------|----------------|--------------------------|
| | SSE | R ² | p | SSE | R ² | p |
| 0–10 | 0.1171 | 0.913 | $1.56 \times 10^{-29} *$ | 0.6394 | 0.854 | $7.39 \times 10^{-75} *$ |
| 10–20 | 0.1281 | 0.908 | $7.82 \times 10^{-29} *$ | 0.6687 | 0.852 | $3.12 \times 10^{-74} *$ |
| 20–30 | 0.1357 | 0.902 | $4.65 \times 10^{-28} *$ | 0.6588 | 0.853 | $1.81 \times 10^{-74} *$ |
| 30–40 | 0.1508 | 0.893 | $5.70 \times 10^{-27} *$ | 0.6262 | 0.861 | $8.80 \times 10^{-77} *$ |
| 40–50 | 0.1443 | 0.900 | $9.82 \times 10^{-28} *$ | 0.5891 | 0.873 | $1.78 \times 10^{-80} *$ |
| 50–60 | 0.1436 | 0.899 | $1.17 \times 10^{-27} *$ | 0.5749 | 0.876 | $2.69 \times 10^{-81} *$ |
| 60–70 | 0.1409 | 0.900 | $9.73 \times 10^{-28} *$ | 0.567 | 0.878 | $6.84 \times 10^{-82} *$ |
| 70–80 | 0.1304 | 0.909 | $5.84 \times 10^{-29} *$ | 0.5479 | 0.884 | $6.77 \times 10^{-84} *$ |
| 80–90 | 0.1292 | 0.906 | $1.43 \times 10^{-28} *$ | 0.5485 | 0.880 | $1.26 \times 10^{-82} *$ |
| 90–100 | 0.1263 | 0.910 | $4.05 \times 10^{-29} *$ | 0.5258 | 0.887 | $7.19 \times 10^{-85} *$ |

* Passed the hypothesis test with significance level $\alpha = 0.01$.

3.4. Residual Analysis

The precipitation and temperature data after impoundment were input into the regression model before impoundment to obtain the predicted NDVI. Then, the residuals between the predicted value and observed value were calculated. The linear regression model was established with time as the independent variable and residuals as the dependent variable. The results of different zones are shown in Table 4. Since the residual trends of the 10 zones were roughly similar, the zone of 0–10 km was taken as an example for specific analysis. The residual variation is shown in Figures 8 and 9. The residuals were mostly negative values, with a decreasing trend over time. It passed the hypothesis test of the significance level $\alpha = 0.05$ with slope $k = -6.02981 \times 10^{-4}$ and $p = 7.51 \times 10^{-15}$. Figures 8 and 9 show that the predicted NDVI was usually smaller than the observed value in the 0–10 km zone.

This significant variation trend of residual cannot be explained by temperature and precipitation but can be regarded as the result of impoundment. In other zones, the residual variation trends were also significant, which were about the same as that of the 0–10 km zone. The predicted NDVI was usually less than the observed value in all zones, which indicated that the TGR impoundment might have a partial impact on the increase of NDVI in the study area. However, comparing the linear regression models of the residuals in different zones (Table 4), it was found that the regression coefficients were different, and the trends of the residuals were not completely similar. Therefore, it is speculated that the impact of impoundment on vegetation might be different in different zones.

Table 4. Slopes of residual trends and test results.

| Zones | k (10^{-4}) | p |
|-----------|-------------------|--------------------------|
| 0–10 km | −6.030 | 7.51×10^{-15} * |
| 10–20 km | −6.020 | 2.09×10^{-14} * |
| 20–30 km | −6.015 | 8.28×10^{-14} * |
| 30–40 km | −6.006 | 1.83×10^{-13} * |
| 40–50 km | −6.004 | 2.73×10^{-13} * |
| 50–60 km | −5.999 | 2.13×10^{-13} * |
| 60–70 km | −5.997 | 2.62×10^{-13} * |
| 70–80 km | −6.006 | 5.72×10^{-13} * |
| 80–90 km | −6.005 | 3.59×10^{-13} * |
| 90–100 km | −6.007 | 4.06×10^{-13} * |

* Passed the hypothesis test with significance level $\alpha = 0.01$.

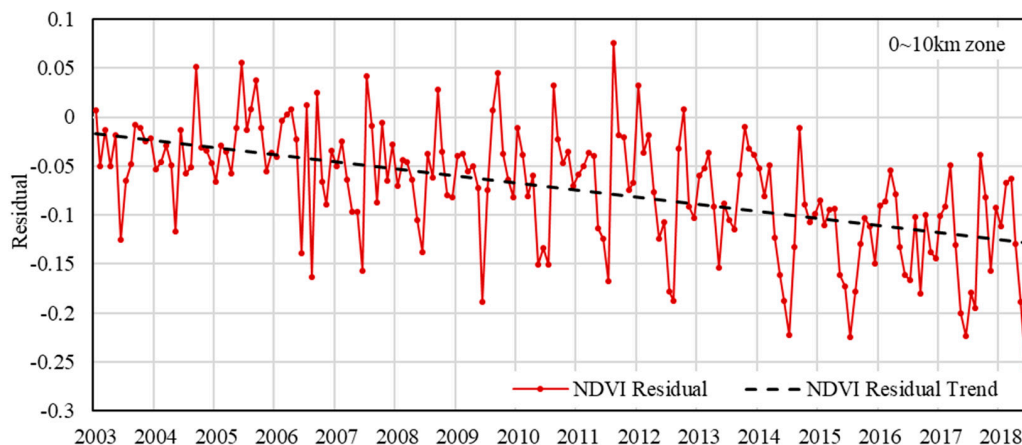


Figure 8. NDVI residuals and residual trend after water impoundment.

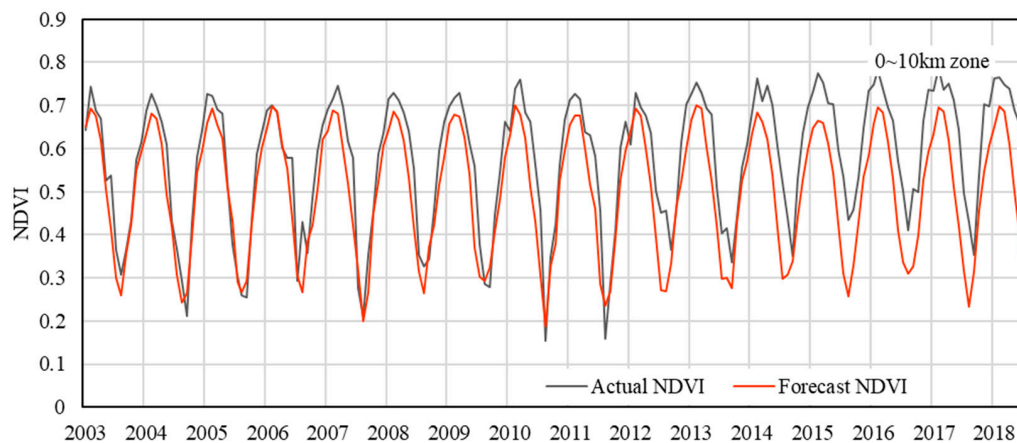


Figure 9. Observed and predicted value of NDVI after impoundment.

3.5. Sensitivity Analysis

To ascertain the evolution of the NDVI–climate response relationship before and after TGR impoundment, the partial derivatives of Equation (5) were calculated and used as a sensitivity index (SI) to characterize the vegetation’s sensitivity to temperature or precipitation. When SI is positive, it indicates that the change direction of vegetation is consistent with that of temperature/precipitation. When SI is negative, it indicates that the change direction of vegetation is opposite to that of temperature/precipitation.

$$SI_x = f'_x = p_1 + 2p_3x + p_4y \quad (10)$$

$$SI_y = f'_y = p_2 + p_4x \quad (11)$$

where x represents temperature, y represents precipitation, f'_x is the partial derivative to x and f'_y is the partial derivative to y . SI_x represents the sensitivity of vegetation to temperature and SI_y represents the sensitivity of vegetation to precipitation.

The absolute value of the difference between the sensitivity index before impoundment and after impoundment was taken as the sensitivity variation index (SVI), calculated through Equations (12) and (13), and used to observe the variation of the vegetation sensitivity to temperature/precipitation between before and after water impoundment.

$$SVI_x = SI_{x2} - SI_{x1} \quad (12)$$

$$SVI_y = SI_{y2} - SI_{y1} \quad (13)$$

where SI_{x1} is the sensitivity of vegetation to temperature before impoundment, SI_{x2} is the sensitivity of vegetation to temperature after impoundment, SI_{y1} is the sensitivity of vegetation to precipitation before impoundment and SI_{y2} is the sensitivity of vegetation to precipitation after impoundment.

From Equation (10), it can be indicated that the sensitivity of vegetation to temperature was affected by precipitation and temperature. Assuming three types of precipitation scenarios (PRE = 100, 200 and 300 mm), the specific analysis based on the zone 0–10 km was carried out. As shown in Figures 10–12, there was a threshold T_c (marked by a red dashed line) in the temperature. When the temperature $T < T_c$, the SI after impoundment was higher than that before impoundment, and the SVI decreased with temperature increasing; when $T > T_c$, the SI after impoundment was lower than that before impoundment, and the SVI increased with the temperature increasing. Under different precipitation scenarios, the temperature threshold was different, and T_c increased with precipitation increasing. As shown in Figures 10–12, the temperature increased and then the SI gradually decreased. The trends of vegetation’s sensitivity to temperature were roughly similar in different zones while temperature thresholds were different, as shown in Table 5.

Table 5. SI of NDVI–temperature and temperature thresholds.

| Zones | Before Impoundment | | | After Impoundment | | | Tc (°C) | | |
|--------|--------------------|-------------------------|------------------------|-------------------|-------------------------|------------------------|-----------------|-----------------|-----------------|
| | p_1 | $2p_3$ (10^{-5}) | p_4 (10^{-6}) | p_1 | $2p_3$ (10^{-4}) | p_4 (10^{-5}) | Pre = 100 mm | Pre = 200 mm | Pre = 300 mm |
| 0–10 | 0.026 | −50.2 | 4.764 | 0.040 | −16.50 | 5.065 | 16.44 | 20.43 | 24.43 |
| 10–20 | 0.025 | −40.58 | 1.527 | 0.041 | −16.77 | 5.578 | 16.41 | 20.68 | 24.95 |
| 20–30 | 0.023 | −20.88 | 1.035 | 0.039 | −15.60 | 5.457 | 16.1 | 20.06 | 24.02 |
| 30–40 | 0.022 | −13.89 | −0.329 | 0.038 | −14.45 | 5.175 | 16.02 | 20.01 | 24 |
| 40–50 | 0.022 | −15.30 | 3.680 | 0.038 | −14.34 | 5.442 | 16.18 | 20.14 | 24.1 |
| 50–60 | 0.023 | −17.54 | 4.098 | 0.037 | −13.82 | 5.274 | 16.22 | 20.25 | 24.29 |
| 60–70 | 0.022 | −14.22 | 5.334 | 0.036 | −13.19 | 5.072 | 16.18 | 20.04 | 23.9 |
| 70–80 | 0.021 | −8.20 | 5.491 | 0.035 | −12.23 | 4.889 | 16.03 | 19.84 | 23.64 |
| 80–90 | 0.021 | −7.39 | 5.806 | 0.035 | −11.72 | 4.53 | 16.16 | 19.75 | 23.35 |
| 90–100 | 0.021 | −7.93 | 4.280 | 0.035 | −11.70 | 4.444 | 16.24 | 19.93 | 23.61 |

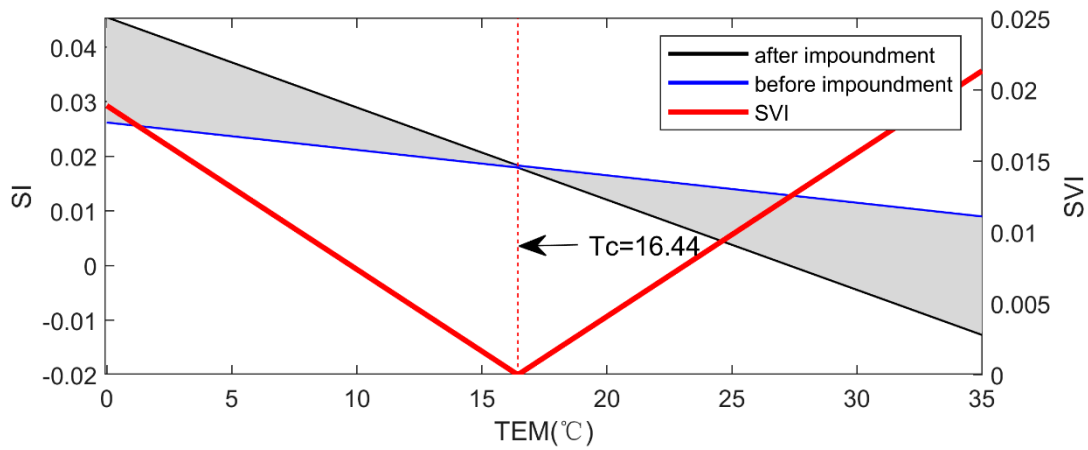


Figure 10. The sensitivity index (SI) and sensitivity variation index (SVI) for the NDVI-temperature response in 0–10 km zone (PRE = 100 mm).

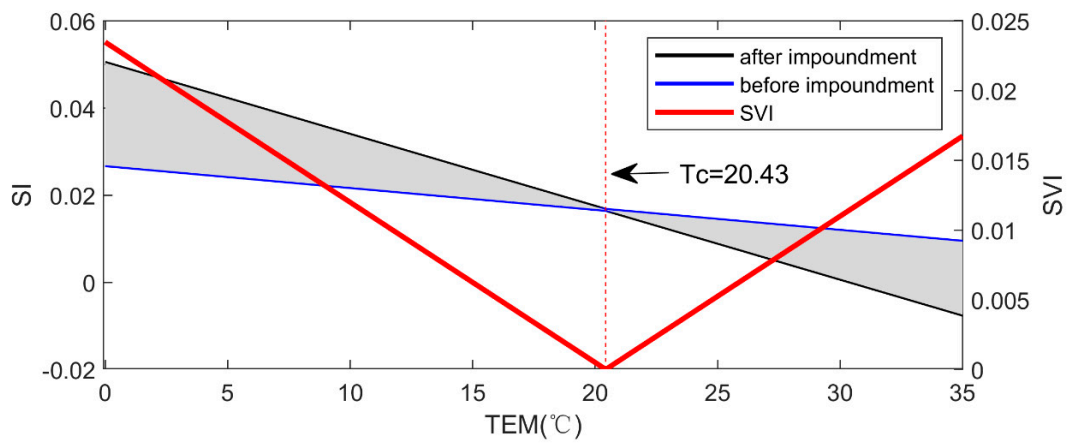


Figure 11. The sensitivity index (SI) and sensitivity variation index (SVI) for the NDVI-temperature response in 0–10 km zone (PRE = 200 mm).

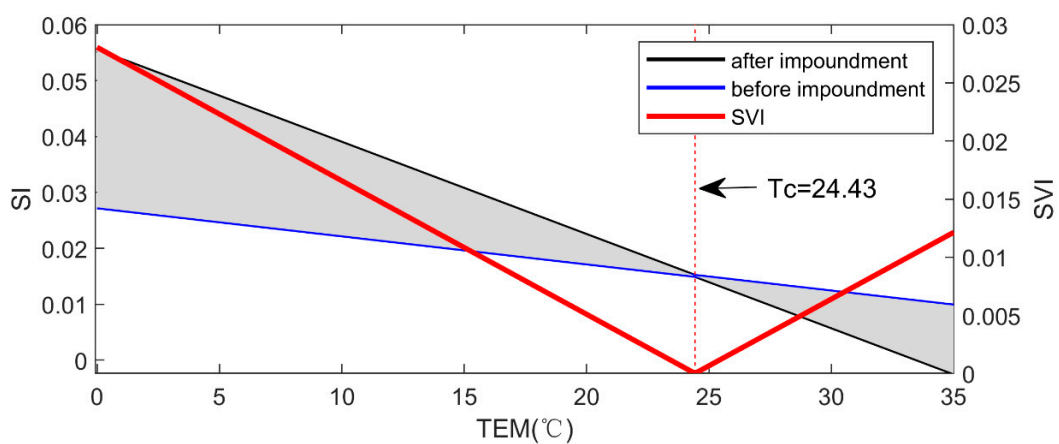


Figure 12. The sensitivity index (SI) and sensitivity variation index (SVI) for the NDVI-temperature response in 0–10 km zone (PRE = 300 mm).

The sensitivity of vegetation to precipitation was affected by temperature. There was a threshold T_c (marked by a red dashed line) in the temperature, as shown in Figure 13. When $T < T_c$, the SI before water impoundment was higher than that after impoundment, and the SVI decreased with temperature increasing; when $T > T_c$, the SI before water impoundment was lower than that after

impoundment, and the SVI increased with the temperature increasing. As the temperature increased, the SI gradually increased. The trends of vegetation's sensitivity to precipitation were roughly similar in different zones while temperature thresholds were different, as shown in Table 6.

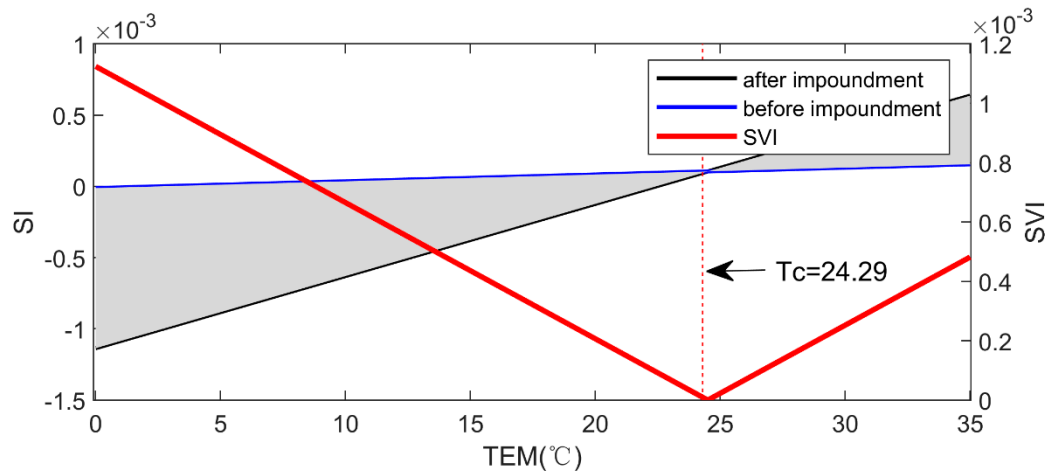


Figure 13. The sensitivity index (SI) and sensitivity variation index (SVI) for the NDVI–precipitation response in 0–10 km zones.

Table 6. SI of NDVI–precipitation and temperature thresholds.

| Zones | Before Impoundment | | After Impoundment | | Tc (°C) |
|--------|---------------------|---------------------|---------------------|---------------------|---------|
| | p_2 (10^{-5}) | p_4 (10^{-6}) | p_2 (10^{-3}) | p_4 (10^{-5}) | |
| 0–10 | −1.176 | 4.764 | −1.136 | 5.065 | 24.29 |
| 10–20 | 1.871 | 1.527 | −1.288 | 5.578 | 23.91 |
| 20–30 | −2.125 | 1.035 | −1.278 | 5.457 | 23.29 |
| 30–40 | −2.628 | −0.329 | −1.231 | 5.175 | 22.95 |
| 40–50 | −12.73 | 3.680 | −1.298 | 5.442 | 22.88 |
| 50–60 | −14.48 | 4.098 | −1.261 | 5.274 | 22.75 |
| 60–70 | −18.55 | 5.334 | −1.210 | 5.072 | 22.36 |
| 70–80 | −18.27 | 5.491 | −1.150 | 4.889 | 22.06 |
| 80–90 | −18.96 | 5.806 | −1.087 | 4.530 | 22.47 |
| 90–100 | −14.87 | 4.280 | −1.075 | 4.444 | 22.82 |

In summary, it was found by comparing SI_x (Figures 10–12) and SI_y (Figure 13) that the sensitivity of vegetation to temperature was higher than that to precipitation, meaning that vegetation was more sensitive to changes in thermal factors [70]. It can be seen from the vegetation–climate regression model and Figure 13 that, while a slight decrease in precipitation can increase the NDVI at low temperature, moderate increase in precipitation can increase the NDVI at high temperature. That is, hot and humid conditions will be more conducive to vegetation growth. Moreover, after TGR impoundment, the variation trend of vegetation's sensitivity to temperature or precipitation was slightly more obvious than that before impoundment. It can be suggested that impoundment might have some effects on the vegetation's sensitivity to climate.

3.6. Difference Analysis

To characterize the difference in the response of NDVI to climate between before and after impoundment, a difference index (DI) was defined as Equations (14) and (15), and calculated in different zones, as shown Figure 14.

$$DI = \frac{|f_2(\alpha, \beta) - f_1(\alpha, \beta)|}{f_1(\alpha, \beta)} \quad (14)$$

$$[\alpha, \beta] = \operatorname{argmax}_{x, y} |f_2(x, y) - f_1(x, y)| \quad (15)$$

where $f_1(x, y)$ is the response of NDVI to temperature and precipitation before water impoundment, $f_2(x, y)$ is the response of NDVI to temperature and precipitation after water impoundment and $[\alpha, \beta]$ is the value of x and y when the absolute value of the difference between function before and after water impoundment is maximum.

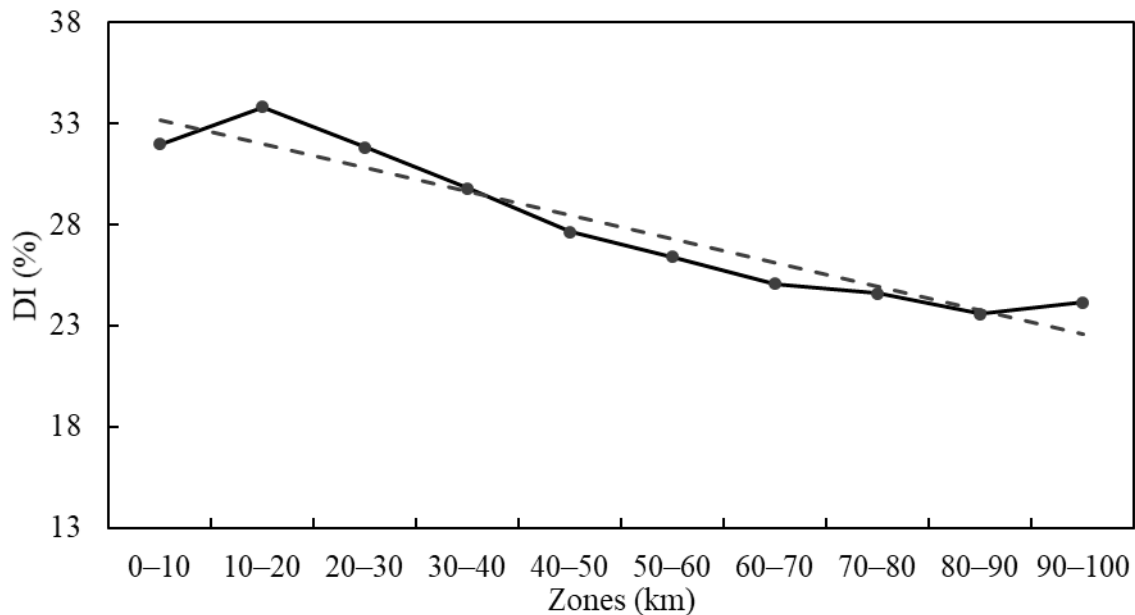


Figure 14. The difference index (DI) describing the change of NDVI–climate response in different zones.

As shown in Figure 14, the DI, which indicates the difference in the pattern of vegetation response to climate between before and after water impoundment, showed a decreasing trend. It can be suggested that vegetation's response to climate was affected by impoundment, and the degree varied by the distance from subarea to TGR, following a rule that the distance increased and then the impact degree decreased.

4. Discussion

Vegetation in most areas showed an increasing trend (Figure 2), while, in Sichuan Basin or the lower reaches of the Yangtze River, vegetation decreased insignificantly or significantly. Urban construction land increased in Sichuan Basin, Chongqing, the middle and lower reaches of the Yangtze River and other places (Figure 3). Combining Figures 2 and 3 to speculate, urbanization and intensive population activities may be the reasons for the heterogeneous distribution of vegetation evolution. Furthermore, the relationship between NDVI and precipitation was weaker than that between NDVI and temperature, and the relationships varied by region.

Combining the vegetation–climate regression model and the sensitivity of vegetation to temperature (Figures 10–12), it can be seen that NDVI will increase when the temperature increases, but it will decrease when temperature exceeds a certain limit. The response mechanism of vegetation activity to temperature is mainly reflected in the degree of warming influence on the processes of photosynthesis and respiration. Moderate warming can have a positive effect on the enhancement of vegetation activity process. However, excessively high temperature will adversely affect the vegetation activity process. As excessive increase in temperature may accelerate the evaporation of soil and form dryness trends, the vegetation will prevent itself from losing water by reducing leaf area and light saturation point, resulting in a corresponding reduction in vegetation coverage and a limited photosynthesis rate [71]. On the other hand, the rising temperature increases the rate of autotrophic respiration and

transpiration of vegetation, accelerates the consumption of organic matter and leads to a reduction in the net productivity, resulting in the inhibition of vegetation activity.

According to the vegetation–climate regression model and the sensitivity of vegetation to precipitation (Figure 13), the observation that precipitation has promotion effect and inhibition effect on vegetation growth can be made. Water participates in physiological and biochemical processes such as photosynthesis and transpiration of vegetation. Many nutrients and minerals in the soil can only be absorbed by plants when dissolved in water. Therefore, increasing precipitation will lead to an increase in photosynthetic rate and organic matter production in vegetation and promote vegetation activities such as growth and cover [72]. However, when the precipitation exceeds the requirement for vegetation, it may also adversely affect vegetation activities such as growth and development indirectly by reducing radiation and increasing relative humidity.

The sensitivity analysis results in Section 3.5 show that the sensitivity of vegetation to temperature was higher than that of vegetation to precipitation. From a geographical perspective, the study area is located in the subtropical monsoon climate and humid zone, with abundant precipitation, suitable temperature, high soil moisture and small evaporation. Thus, vegetation activity is not restricted by water, and the increase in temperature is conducive to the extension of vegetation growth season and accumulation of dry matter quality [73].

Residual analysis method and SI and DI indicator method were used to distinguish and quantify the impact of TGR impoundment on the vegetation–climate response relationship. The results in Figure 14 show that the vegetation–climate relationship may be affected by impoundment, and impact degree decreased as the distance from subarea to TGR increased. Judging from the results, the impact of TGR impoundment may be the reason for vegetation–climate response relationship variation. However, how TGR impoundment affected the relationship is still unknown. In addition, residual analysis method and SI and DI indicator method have certain limitations when they are used to study the impact of human activities. It is more difficult to build a perfectly ideal model without the influence of human activities, but focusing on a specific impact will make it more feasible to build a model that is not affected by this specific impact. Improving methods to make it more widely used is also one of the directions that can be studied in the future.

5. Conclusions

This study used partial correlation analysis, grid point analysis, residual analysis and Mann–Kendall test methods to analyze and quantify the impact of TGR impoundment on the vegetation–climate relationship in the TGRR and its 100-km buffer zone, based on SPOT/VEGETATION NDVI and ERA5 datasets during 1998–2018. Two types of index were proposed and compared with residual analysis method to quantify the impact of TGR impoundment on the vegetation–climate relationship. Finally, the conclusion can be drawn as follows:

In the TGRR and its 100-km buffer zones, NDVI in most areas showed a significant increasing trend. However, in Sichuan Basin or the lower reaches of the Yangtze River, intensive human activities might be the reason for NDVI decreasing significantly. The partial correlation coefficients of NDVI–temperature were higher than those of NDVI–precipitation, and the dynamic response of vegetation cover to temperature and precipitation changes had strong spatial heterogeneity. More importantly, temperature was the main driving factor of vegetation cover change.

The multiple polynomial regression, which simplified relationship and explained the physical mechanism, could effectively describe the response of vegetation–climate before and after water impoundment. The residuals between predicted NDVI and the observed value after impoundment were mostly negative and decreased significantly. In other words, observed NDVI was higher than predicted. The significant decreasing residuals that cannot be explained by independent variables (climatic factors: temperature and precipitation) may be caused by impoundment of TGR. The trends of the residuals were not completely similar in different zones, but this difference was not intuitive.

In this study, SI and DI, which are more intuitive and clearer when displaying the results, were proposed, respectively, to describe and quantify the vegetation's sensitivity to climate and the difference between before and after water impoundment. In terms of the sensitivity of vegetation to climate, SI and SVI indices were defined, which can effectively quantify the difference of vegetation–climate response between before and after water impoundment. The sensitivity of vegetation to temperature was affected by precipitation and temperature, while the sensitivity of vegetation to precipitation was affected by temperature. The variation of sensitivity after impoundment was slightly more obvious than that before impoundment, and the direction of this sensitivity variation was related to the temperature threshold. In addition, SI results indicate that vegetation was more sensitive to changes in temperature. Hot and humid conditions will be more conducive to vegetation growth. In terms of the difference in the response of NDVI to climate between before and after water impoundment, the DI results show that water impoundment might have an impact on the response relationship of vegetation to climate, and the impact degree decreased with increasing the distance between subarea and TGR.

Comparing residual analysis method and SI and DI indicator method, it can be found that these two methods are essential to quantify the difference of the vegetation–climate relationship between before and after impoundment to reflect the impact on vegetation. They can both quantify and show the difference before and after the impact, but the residual analysis method showed the impact of impoundment through the significant change trend of the residual, while SI and DI indicators directly showed this impact degree. The results of the residual analysis method are less intuitive compared with those of the SI and DI indicators. In addition, it seems that the SI and DI index methods are more effective when comparing the impact of impoundment on vegetation in different areas. Therefore, it may be desirable to combine the residual analysis method with SI and DI indicator method to better and more comprehensively analyze the impact of human activities. A new idea is provided for the study on the impact of human activities in the future.

This study distinguished and quantified the impact of TGR impoundment on the vegetation–climate response relationship. However, its impact is a complex and far-reaching process, which needs to be further studied to find the mechanism and provide a basis for management and decision-making.

Author Contributions: Project administration, J.Z.; Software, B.J.; Writing—original draft, M.T.; and Writing—review and editing, M.T., J.Z., B.J., S.L. and H.W. All authors have read and agreed to the published version of the manuscript.

Funding: This work was jointly supported by the National Natural Science Foundation of China (grant numbers: U1865202 and 91547208) and the National Key R&D Program of China (grant number: 2016YFC0402205).

Acknowledgments: Special thanks are given to the anonymous reviewers and editors for their constructive comments that greatly enrich the manuscript. The authors acknowledge the providers of SPOT/VEGETATION NDVI (doi:10.12078/2018060602 and 10.12078/2018060601), land use/land cover, and ERA5 reanalysis (doi:10.24381/cds.adbb2d47) data for their valuable and accessible information.

Conflicts of Interest: The authors declare no conflict of interest.

References

1. Sun, W.; Song, X.; Mu, X.; Gao, P.; Wang, F.; Zhao, G. Spatiotemporal vegetation cover variations associated with climate change and ecological restoration in the Loess Plateau. *Agric. For. Meteorol.* **2015**, *209–210*, 87–99. [[CrossRef](#)]
2. Jia, K.; Liang, S.; Zhang, L.; Wei, X.; Yao, Y.; Xie, X. Forest cover classification using Landsat ETM+ data and time series MODIS NDVI data. *Int. J. Appl. Earth Obs. Geoinf.* **2014**, *33*, 32–38. [[CrossRef](#)]
3. Bégué, A.; Vintrou, E.; Ruelland, D.; Claden, M.; Dessay, N. Can a 25-year trend in Soudano-Sahelian vegetation dynamics be interpreted in terms of land use change? A remote sensing approach. *Glob. Environ. Chang.* **2011**, *21*, 413–420. [[CrossRef](#)]
4. Wang, Q.; Zhang, Q.; Zhou, W. Grassland coverage changes and analysis of the driving forces in Maqu County. *Phys. Procedia* **2012**, *33*, 1292–1297. [[CrossRef](#)]

5. De Jong, R.; de Bruin, S.; de Wit, A.; Schaepman, M.E.; Dent, D.L. Analysis of monotonic greening and browning trends from global NDVI time-series. *Remote Sens. Environ.* **2011**, *115*, 692–702. [[CrossRef](#)]
6. Chen, B.; Xu, G.; Coops, N.C.; Ciais, P.; Innes, J.L.; Wang, G.; Myneni, R.B.; Wang, T.; Krzyzanowski, J.; Li, Q.; et al. Changes in vegetation photosynthetic activity trends across the Asia-Pacific region over the last three decades. *Remote Sens. Environ.* **2014**, *144*, 28–41. [[CrossRef](#)]
7. Krishnaswamy, J.; John, R.; Joseph, S. Consistent response of vegetation dynamics to recent climate change in tropical mountain regions. *Glob. Chang. Biol.* **2014**, *20*, 203–215. [[CrossRef](#)]
8. Tousignant, M.É.; Pellerin, S.; Brisson, J. The relative impact of human disturbances on the vegetation of a large wetland complex. *Wetlands* **2010**, *30*, 333–344. [[CrossRef](#)]
9. Root, T.L.; Price, J.T.; Hall, K.R.; Schneider, S.H.; Rosenzweig, C.; Pounds, J.A. Fingerprints of global warming on wild animals and plants. *Nature* **2003**, *421*, 57–60. [[CrossRef](#)]
10. Piao, S.; Nan, H.; Huntingford, C.; Ciais, P.; Friedlingstein, P.; Sitch, S.; Peng, S.; Ahlström, A.; Canadell, J.G.; Cong, N.; et al. Evidence for a weakening relationship between interannual temperature variability and northern vegetation activity. *Nat. Commun.* **2014**, *5*, 6018. [[CrossRef](#)]
11. Liu, Y.Y.; van Dijk, A.I.J.M.; McCabe, M.F.; Evans, J.P.; de Jeu, R.A.M. Global vegetation biomass change (1988–2008) and attribution to environmental and human drivers. *Glob. Ecol. Biogeogr.* **2013**, *22*, 692–705. [[CrossRef](#)]
12. Strengers, B.J.; Müller, C.; Schaeffer, M.; Haarsma, R.J.; Severijns, C.; Gerten, D.; Schaphoff, S.; Van Den Houdt, R.; Oostenrijk, R. Assessing 20th century climate-vegetation feedbacks of land-use change and natural vegetation dynamics in a fully coupled vegetation-climate model. *Int. J. Climatol.* **2010**, *30*, 2055–2065. [[CrossRef](#)]
13. Xu, G.; Zhang, H.; Chen, B.; Zhang, H.; Innes, J.L.; Wang, G.; Yan, J.; Zheng, Y.; Zhu, Z.; Myneni, R.B. Changes in vegetation growth dynamics and relations with climate over China's landmass from 1982 to 2011. *Remote Sens.* **2014**, *6*, 3263–3283. [[CrossRef](#)]
14. Huang, K.; Zhang, Y.; Zhu, J.; Liu, Y.; Zu, J.; Zhang, J. The influences of climate change and human activities on vegetation dynamics in the Qinghai-Tibet plateau. *Remote Sens.* **2016**, *8*, 876. [[CrossRef](#)]
15. Horion, S.; Cornet, Y.; Erpicum, M.; Tychon, B. Studying interactions between climate variability and vegetation dynamic using a phenology based approach. *Int. J. Appl. Earth Obs. Geoinf.* **2012**, *20*, 20–32. [[CrossRef](#)]
16. Zhao, X.; Tan, K.; Zhao, S.; Fang, J. Changing climate affects vegetation growth in the arid region of the northwestern China. *J. Arid Environ.* **2011**, *75*, 946–952. [[CrossRef](#)]
17. Xin, Z.B.; Xu, J.X.; Zheng, W. Spatiotemporal variations of vegetation cover on the Chinese Loess Plateau (1981–2006): Impacts of climate changes and human activities. *Sci. China Ser. D Earth Sci.* **2008**, *51*, 67–78. [[CrossRef](#)]
18. Xie, B.; Jia, X.; Qin, Z.; Shen, J.; Chang, Q. Vegetation dynamics and climate change on the Loess Plateau, China: 1982–2011. *Reg. Environ. Chang.* **2016**, *16*, 1583–1594. [[CrossRef](#)]
19. Xu, X.; Chen, H.; Levy, J.K. Spatiotemporal vegetation cover variations in the Qinghai-Tibet Plateau under global climate change. *Chin. Sci. Bull.* **2008**, *53*, 915–922. [[CrossRef](#)]
20. Kong, D.; Zhang, Q.; Singh, V.P.; Shi, P. Seasonal vegetation response to climate change in the Northern Hemisphere (1982–2013). *Glob. Planet. Chang.* **2017**, *148*, 1–8. [[CrossRef](#)]
21. Piao, S.; Mohammat, A.; Fang, J.; Cai, Q.; Feng, J. NDVI-based increase in growth of temperate grasslands and its responses to climate changes in China. *Glob. Environ. Chang.* **2006**, *16*, 340–348. [[CrossRef](#)]
22. Mohammat, A.; Wang, X.; Xu, X.; Peng, L.; Yang, Y.; Zhang, X.; Myneni, R.B.; Piao, S. Drought and spring cooling induced recent decrease in vegetation growth in Inner Asia. *Agric. For. Meteorol.* **2013**, *178*–179, 21–30. [[CrossRef](#)]
23. Xu, H.J.; Wang, X.P.; Yang, T.B. Trend shifts in satellite-derived vegetation growth in Central Eurasia, 1982–2013. *Sci. Total Environ.* **2017**, *579*, 1658–1674. [[CrossRef](#)] [[PubMed](#)]
24. Notaro, M.; Chen, G.; Yu, Y.; Wang, F.; Tawfik, A. Regional climate modeling of vegetation feedbacks on the Asian-Australian monsoon systems. *J. Clim.* **2017**, *30*, 1553–1582. [[CrossRef](#)]
25. Johannsen, F.; Ermida, S.; Martins, J.P.A.; Trigo, I.F.; Nogueira, M.; Dutra, E. Cold bias of ERA5 summertime daily maximum land surface temperature over Iberian Peninsula. *Remote Sens.* **2019**, *11*, 2570. [[CrossRef](#)]

26. Nogueira, M.; Albergel, C.; Boussetta, S.; Johannsen, F.; Trigo, I.; Ermida, S.; Martins, J.; Dutra, E. Role of vegetation in representing land surface temperature in the CHTESSEL (CY45R1) and SURFEX-ISBA (v8.1) land surface models: A case study over Iberia. *Geosci. Model. Dev. Discuss.* **2020**, 1–29. [[CrossRef](#)]
27. Zhang, Y.; Zhang, C.; Wang, Z.; Chen, Y.; Gang, C.; An, R.; Li, J. Vegetation dynamics and its driving forces from climate change and human activities in the Three-River Source Region, China from 1982 to 2012. *Sci. Total Environ.* **2016**, 563–564, 210–220. [[CrossRef](#)]
28. Hua, W.; Chen, H.; Zhou, L.; Xie, Z.; Qin, M.; Li, X.; Ma, H.; Huang, Q.; Sun, S. Observational quantification of climatic and human influences on vegetation greening in China. *Remote Sens.* **2017**, 9, 425. [[CrossRef](#)]
29. Brandt, M.; Rasmussen, K.; Peñuelas, J.; Tian, F.; Schurgers, G.; Verger, A.; Mertz, O.; Palmer, J.R.B.; Fensholt, R. Human population growth offsets climate-driven increase in woody vegetation in sub-Saharan Africa. *Nat. Ecol. Evol.* **2017**, 1, 0081. [[CrossRef](#)]
30. Li, S.; Yan, J.; Liu, X.; Wan, J. Response of vegetation restoration to climate change and human activities in Shaanxi-Gansu-Ningxia Region. *J. Geogr. Sci.* **2013**, 23, 98–112. [[CrossRef](#)]
31. Li, S.; Yang, S.; Liu, X.; Liu, Y.; Shi, M. NDVI-based analysis on the influence of climate change and human activities on vegetation restoration in the shaanxi-gansu-ningxia region, central China. *Remote Sens.* **2015**, 7, 11163–11182. [[CrossRef](#)]
32. Wang, H.; Liu, G.; Li, Z.; Ye, X.; Fu, B.; Lv, Y. Impacts of Drought and Human Activity on Vegetation Growth in the Grain for Green Program Region, China. *Chin. Geogr. Sci.* **2018**, 28, 470–481. [[CrossRef](#)]
33. Zhang, J.; Zhengjun, L.; Xiaoxia, S. Changing landscape in the Three Gorges Reservoir Area of Yangtze River from 1977 to 2005: Land use/land cover, vegetation cover changes estimated using multi-source satellite data. *Int. J. Appl. Earth Obs. Geoinf.* **2009**, 11, 403–412. [[CrossRef](#)]
34. Evans, J.; Geerken, R. Discrimination between climate and human-induced dryland degradation. *J. Arid Environ.* **2004**, 57, 535–554. [[CrossRef](#)]
35. Herrmann, S.M.; Anyamba, A.; Tucker, C.J. Recent trends in vegetation dynamics in the African Sahel and their relationship to climate. *Glob. Environ. Chang.* **2005**, 15, 394–404. [[CrossRef](#)]
36. Wessels, K.J.; van den Bergh, F.; Scholes, R.J. Limits to detectability of land degradation by trend analysis of vegetation index data. *Remote Sens. Environ.* **2012**, 125, 10–22. [[CrossRef](#)]
37. Jiang, L.; Jiapaer, G.; Bao, A.; Guo, H.; Ndayisaba, F. Vegetation dynamics and responses to climate change and human activities in Central Asia. *Sci. Total Environ.* **2017**, 599–600, 967–980. [[CrossRef](#)]
38. Sun, Y.; Yang, Y.; Zhang, L.; Wang, Z. The relative roles of climate variations and human activities in vegetation change in North China. *Phys. Chem. Earth* **2015**, 87–88, 67–78. [[CrossRef](#)]
39. Wang, J.; Wang, K.; Zhang, M.; Zhang, C. Impacts of climate change and human activities on vegetation cover in hilly southern China. *Ecol. Eng.* **2015**, 81, 451–461. [[CrossRef](#)]
40. Wen, Z.; Wu, S.; Chen, J.; Lü, M. NDVI indicated long-term interannual changes in vegetation activities and their responses to climatic and anthropogenic factors in the Three Gorges Reservoir Region, China. *Sci. Total Environ.* **2017**, 574, 947–959. [[CrossRef](#)]
41. Caesagtgp, S. *Staged Assessment Report of the Three Gorges Project (Comprehensive Volume)*; Chinese Water Power Press: Beijing, China, 2010.
42. Wu, J.; Huang, J.; Han, X.; Gao, X.; He, F.; Jiang, M.; Jiang, Z.; Primack, R.B.; Shen, Z. The Three Gorges Dam: An ecological perspective. *Front. Ecol. Environ.* **2004**, 2, 241–248. [[CrossRef](#)]
43. Kerr, J.T.; Ostrovsky, M. From space to species: Ecological applications for remote sensing. *Trends Ecol. Evol.* **2003**, 18, 299–305. [[CrossRef](#)]
44. Turner, W.; Spector, S.; Gardiner, N.; Fladeland, M.; Sterling, E.; Steininger, M. Remote sensing for biodiversity science and conservation. *Trends Ecol. Evol.* **2003**, 18, 306–314. [[CrossRef](#)]
45. Yao, B.; Teng, S.; Lai, R.; Xu, X.; Yin, Y.; Shi, C.; Liu, C. Can atmospheric reanalyses (CRA and ERA5) represent cloud spatiotemporal characteristics? *Atmos. Res.* **2020**, 244, 105091. [[CrossRef](#)]
46. Lyu, F.; Tang, G.; Behrangi, A.; Wang, T.; Tan, X.; Ma, Z.; Xiong, W. Precipitation Merging Based on the Triple Collocation Method Across Mainland China. *IEEE Trans. Geosci. Remote Sens.* **2020**, 1–16. [[CrossRef](#)]
47. Yang, J.; Gong, P.; Fu, R.; Zhang, M.; Chen, J.; Liang, S.; Xu, B.; Shi, J.; Dickinson, R. The role of satellite remote sensing in climate change studies. *Nat. Clim. Chang.* **2013**, 3, 875–883. [[CrossRef](#)]
48. Wang, X.; Yang, F.; Gao, X.; Wang, W.; Zha, X. Evaluation of Forest Damaged Area and Severity Caused by Ice-snow Frozen Disasters over Southern China with Remote Sensing. *Chin. Geogr. Sci.* **2019**, 29, 405–416. [[CrossRef](#)]

49. Di, L.; Yu, E.; Shrestha, R.; Lin, L. DVDI: A new remotely sensed index for measuring vegetation damage caused by natural disasters. *Int. Geosci. Remote Sens. Symp.* **2018**, *2018*, 9067–9069. [[CrossRef](#)]
50. Klisch, A.; Atzberger, C. Operational drought monitoring in Kenya using MODIS NDVI time series. *Remote Sens.* **2016**, *8*, 267. [[CrossRef](#)]
51. Beck, P.S.A.; Atzberger, C.; Høgda, K.A.; Johansen, B.; Skidmore, A.K. Improved monitoring of vegetation dynamics at very high latitudes: A new method using MODIS NDVI. *Remote Sens. Environ.* **2006**, *100*, 321–334. [[CrossRef](#)]
52. Neigh, C.S.R.; Tucker, C.J.; Townshend, J.R.G. North American vegetation dynamics observed with multi-resolution satellite data. *Remote Sens. Environ.* **2008**, *112*, 1749–1772. [[CrossRef](#)]
53. Pettorelli, N.; Vik, J.O.; Mysterud, A.; Gaillard, J.M.; Tucker, C.J.; Stenseth, N.C. Using the satellite-derived NDVI to assess ecological responses to environmental change. *Trends Ecol. Evol.* **2005**, *20*, 503–510. [[CrossRef](#)] [[PubMed](#)]
54. Running, S.W. Estimating Terrestrial Primary Productivity by Combining Remote Sensing and Ecosystem Simulation. *Remote Sens. Biosph. Funct.* **1990**, 65–86. [[CrossRef](#)]
55. Myneni, R.B.; Hall, F.G.; Sellers, P.J.; Marshak, A.L. Interpretation of spectral vegetation indexes. *IEEE Trans. Geosci. Remote Sens.* **1995**, *33*, 481–486. [[CrossRef](#)]
56. Data Center for Resources and Environmental Sciences, Chinese Academy of Sciences. NDVI Spatial Distribution Dataset in China. Available online: <http://www.resdc.cn> (accessed on 11 February 2020).
57. Data Center for Resources and Environmental Sciences, Chinese Academy of Sciences. Land Use/Land Cover Remote Sensing Monitoring Dataset in China. Available online: <http://www.resdc.cn> (accessed on 5 August 2020).
58. Liu, J.; Zhang, Z.; Xu, X.; Kuang, W.; Zhou, W.; Zhang, S.; Li, R.; Yan, C.; Yu, D.; Wu, S.; et al. Spatial patterns and driving forces of land use change in China during the early 21st century. *J. Geogr. Sci.* **2010**, *20*, 483–494. [[CrossRef](#)]
59. Climate Data Store. Available online: <https://cds.climate.copernicus.eu/> (accessed on 16 February 2019).
60. Albergel, C.; Dutra, E.; Munier, S.; Calvet, J.C.; Munoz-Sabater, J.; De Rosnay, P.; Balsamo, G. ERA-5 and ERA-Interim driven ISBA land surface model simulations: Which one performs better? *Hydrol. Earth Syst. Sci.* **2018**, *22*, 3515–3532. [[CrossRef](#)]
61. Nogueira, M. Inter-comparison of ERA-5, ERA-interim and GPCP rainfall over the last 40 years: Process-based analysis of systematic and random differences. *J. Hydrol.* **2020**, *583*, 124632. [[CrossRef](#)]
62. Tarek, M.; Brissette, F.; Arsenaault, R. Evaluation of the ERA5 reanalysis as a potential reference dataset for hydrological modeling over North-America. *Hydrol. Earth Syst. Sci. Discuss.* **2020**, *24*, 2527–2544. [[CrossRef](#)]
63. Tang, G.; Clark, M.P.; Papalexiou, S.M.; Ma, Z.; Hong, Y. Have satellite precipitation products improved over last two decades? A comprehensive comparison of GPM IMERG with nine satellite and reanalysis datasets. *Remote Sens. Environ.* **2020**, *240*, 111697. [[CrossRef](#)]
64. Yang, H.; He, C.; Wang, Z.; Shao, W. Reliability Analysis of European ERA5 Water Vapor Content Based on Ground-based GPS in China. *Atlantis Press* **2019**, *89*, 44–49. [[CrossRef](#)]
65. Zhang, W.; Zhang, H.; Liang, H.; Lou, Y.; Cai, Y.; Cao, Y.; Zhou, Y.; Liu, W. On the suitability of ERA5 in hourly GPS precipitable water vapor retrieval over China. *J. Geod.* **2019**, *93*, 1897–1909. [[CrossRef](#)]
66. Mann, H.B. Nonparametric tests against trend. *Econometrica* **1945**, *13*, 245. [[CrossRef](#)]
67. Kendall, M.G. Rank correlation methods. *Biometrika* **1957**, *44*, 298. [[CrossRef](#)]
68. Xiang, F.; Wang, L.; Yao, R.; Niu, Z. The characteristics of climate change and response of vegetation in three gorges reservoir area. *Earth Sci.* **2018**, *43*, 42–52. (In Chinese) [[CrossRef](#)]
69. Zhang, L.; Shen, J.; Liu, X.; Zhu, W. Vegetation changes in the three gorges reservoir area from 2001 to 2016 and the analysis of its climate driving factors. *Geogr. Geo Inf. Sci.* **2019**, *35*, 38–46. (In Chinese) [[CrossRef](#)]
70. Clifford, M.J.; Royer, P.D.; Cobb, N.S.; Breshears, D.D.; Ford, P.L. Precipitation thresholds and drought-induced tree die-off: Insights from patterns of *Pinus edulis* mortality along an environmental stress gradient. *New Phytol.* **2013**, *200*, 413–421. [[CrossRef](#)]
71. Zhang, K.; Kimball, J.S.; Nemani, R.R.; Running, S.W.; Hong, Y.; Gourley, J.J.; Yu, Z. Vegetation Greening and Climate Change Promote Multidecadal Rises of Global Land Evapotranspiration. *Sci. Rep.* **2015**, *5*, 15956. [[CrossRef](#)]

72. Gourджи, S.M.; Sibley, A.M.; Lobell, D.B. Global crop exposure to critical high temperatures in the reproductive period: Historical trends and future projections. *Environ. Res. Lett.* **2013**, *8*, 024041. [[CrossRef](#)]
73. Jiao, K.; Gao, J.; Wu, S.; Hou, W. Research progress on the response processes of vegetation activity to climate change. *Acta Ecol. Sin.* **2018**, *38*, 2229–2238. (In Chinese) [[CrossRef](#)]



© 2020 by the authors. Licensee MDPI, Basel, Switzerland. This article is an open access article distributed under the terms and conditions of the Creative Commons Attribution (CC BY) license (<http://creativecommons.org/licenses/by/4.0/>).